Science Bulletin 62 (2017) 277–289

Contents lists available at ScienceDirect

Science Bulletin

journal homepage: www.elsevier.com/locate/scib

Article

# Simple and cost-effective methods for precise analysis of trace element abundances in geological materials with ICP-MS

Shuo Chen [a,b,c,*], Xiaohong Wang [a,b], Yaoling Niu [a,b,d,*], Pu Sun [a,b,c], Meng Duan [e], Yuanyuan Xiao [a,b], Pengyuan Guo [a,b], Hongmei Gong [a,b], Guodong Wang [a,b], Qiqi Xue [e]

[a] Institute of Oceanology, Chinese Academy of Sciences, Qingdao 266071, China
[b] Laboratory for Marine Geology, Qingdao National Laboratory for Marine Science and Technology, Qingdao 266061, China
[c] University of Chinese Academy of Sciences, Beijing 100049, China
[d] Department of Earth Sciences, Durham University, Durham DH1 3LE, UK
[e] School of Earth Science and Mineral Resources, China University of Geosciences, Beijing 100083, China

ARTICLE INFO

*Article history:*
Received 24 October 2016
Received in revised form 24 December 2016
Accepted 26 December 2016
Available online 4 January 2017

*Keywords:*
Inductively coupled plasma mass spectrometry
High-pressure digestion
Oxide and hydroxide interferences
Instrumental drift
Correction methods
Trace elements

ABSTRACT

Inductively coupled plasma mass spectrometry (ICP-MS) is the most commonly used technique to determine the abundances of trace elements in a wide range of geological materials. However, incomplete sample digestion, isobaric interferences and instrumental drift remain obvious problems that must be overcome in order to obtain precise and accurate results. For this reason, we have done many experiments and developed a set of simple, cost-effective and practical methods widely applicable for precise and rapid determination of trace element abundances in geological materials using ICP-MS. Commonly used high-pressure digestion technique is indeed effective in decomposing refractory phases, but this inevitably produces fluoride complexes that create new problems. We demonstrate that the fluoride complexes formed during high-pressure digestion can be readily re-dissolved using high-pressure vessel at 190 °C for only 2 h for 50 mg sample. In the case of isobaric interferences, although oxide (e.g., $MO^+/M^+$) and hydroxide (e.g., $MOH^+/M^+$) productivity is variable between runs, the $(MO^+/M^+)/(CeO^+/Ce^+)$ and $(MOH^+/M^+)/(CeO^+/Ce^+)$ ratios remain constant, making isobaric interference correction for all other elements of interest straightforward, for which we provide an easy-to-use off-line procedure. We also show that mass-time-intensity drift curve is smooth as recognized previously, for which the correction can be readily done by analyzing a quality-control (QC) solution and using off-line Excel VBA procedure without internal standards. With these methods, we can produce data in reasonable agreement with recommended values of international rock reference standards with a relative error of <8% and precision generally better than 5%. Importantly, compared to the widely used analytical practice, we can effectively save >60% of time (e.g., <24 h vs. >60 h).



## 1. Introduction

Inductively coupled plasma mass spectrometry (ICP-MS) has been widely used for analyzing trace element abundances in all sorts of geological materials, as it can rapidly analyze most elements with very low detection limits and relatively simple sample preparation [1,2]. Although laser-ablation ICP-MS (or LA-ICP-MS) has made it possible for *in situ* analysis on solid samples directly, most applications still require acid-solution analysis [3]. In fact, the three-orders of magnitude lower detection limit (vs. LA-ICP-MS) makes the solution ICP-MS analysis indispensable for elements of low and ultra-low abundances (low ppb and ppt levels). For geological samples, complete decomposition is thus prerequisite for high quality solution-ICP-MS analysis [4]. Also, the analytical precision and accuracy also depend on instrument conditions and methods employed [5]. While the ICP-MS technique has been significantly matured over the past ~30 years, various isobaric interferences as the result of sample introduction and transport to the ICP remain one of the problems to be monitored and overcome [6].

In this paper, we do not intend to review the development of ICP-MS but to briefly document the common problems, and offer a set of simple, cost-effective and practical methods for both

* Corresponding authors.
*E-mail addresses:* chenshuo528@foxmail.com (S. Chen), yaoling.niu@foxmail.com (Y. Niu).

http://dx.doi.org/10.1016/j.scib.2017.01.004
2095-9273/

sample digestion and interference corrections with which we demonstrate to provide rapid analysis of trace element abundances with high precision and accuracy in geological materials using ICP-MS.

## 2. Experiments

### 2.1. Instrumentation

The instrument used is an Agilent 7900 ICP-MS instrument (Agilent Technologies, Tokyo, Japan) in the Laboratory of Ocean Lithosphere and Mantle Dynamics, Institute of Oceanology, Chinese Academy of Sciences. Detailed operating conditions and instrumental parameters are given in Table 1. The instrument was first optimized to obtain maximum signal intensities for $^{7}$Li, $^{89}$Y, $^{140}$Ce and $^{205}$Tl using a 1 μg $L^{-1}$ tuning solution containing Li, Y, Co, Ce, Mg and Tl, while keeping the formation of oxides $^{140}CeO^{+}/^{140}Ce^{+}$ and doubly charged species $Ce^{2+}/Ce^{+}$ ratios below 1.2%. A rock solution was then flushed for 30 min before tuning the instrument to minimize the drift. Drift corrections were done by repeated analysis of a rock sample as drift monitor (QC; quality control rock solutions) between every 4 unknown samples without internal standards. The oxide and hydroxide interferences were corrected for using a series of equations described in Section 4. Detailed procedure of instrumental drift correction is discussed and described in Section 5. The memory effect is minimized by manual analysis and observing $^{181}$Ta count levels between samples in a wash solution of 1% Triton X-100 alternated with 2% $HNO_3$.

### 2.2. Reagents

All solutions were prepared using ultra-pure water (18.2 MΩ), which was obtained from a Milli-Q water purification system (Millipore, Bedford, MA, USA). Commercially available nitric acid (68% v/v, GR grade), hydrofluoric acid (40% v/v, GR grade) were further distilled in a sub-boiling distillation system. Hydrochloric acid (36% v/v, MOS grade) were directly used. Four solutions (1, 10, 50 and 100 ng $mL^{-1}$ for all elements) were prepared by gravimetrical dilution from Multi-element Calibration Standard solutions (Agilent Technologies, Tokyo, Japan) as external calibrators. Multi mono-element solutions were prepared from 1 mg $mL^{-1}$ of single element standard solutions (National Center for Analysis and Testing of Steel Materials, China).

**Table 1**
ICP-MS instrumentation and operating conditions.

| Instrument parameters | (Agilent 7900, Agilent Technologies, Tokyo, Japan) |
|---|---|
| Nebuliser | Microflow PFA |
| Torch | Quartz glass torch |
| Spray chamber | Scott double-pass type at 2 °C |
| Sampling depth | 10 mm |
| Sample cone | Nickel, 1.0 mm aperture |
| Skimmer cone | Nickel, 0.45 mm aperture |
| Detector mode | Dual |
| Dwell time per peak | 90 ms |
| Scan type | Peak hopping |
| RF power | 1550 W |
| Plasma gas flow rate | 15 L/min |
| Auxiliary gas flow rate | 1.0 L/min |
| Carrier gas flow rate | 1.05 L/min |
| Sample uptake rate | 0.10 ml/min |
| Isotopes | $^{7}$Li, $^{9}$Be, $^{45}$Sc, $^{47}$Ti, $^{51}$V, $^{53}$Cr, $^{55}$Mn, $^{59}$Co, $^{60}$Ni, $^{63}$Cu, $^{66}$Zn, $^{71}$Ga, $^{85}$Rb, $^{88}$Sr, $^{89}$Y, $^{90}$Zr, $^{93}$Nb, $^{133}$Cs, $^{137}$Ba, $^{139}$La, $^{140}$Ce, $^{141}$Pr, $^{146}$Nd, $^{147}$Sm, $^{151}$Eu, $^{156}$Gd, $^{159}$Tb, $^{163}$Dy, $^{165}$Ho, $^{167}$Er, $^{169}$Tm, $^{173}$Yb, $^{175}$Lu, $^{178}$Hf, $^{181}$Ta, $^{206,207,208}$Pb, $^{232}$Th, $^{238}$U |

## 3. A simple and cost-effective method for geological sample digestion

### 3.1. A brief review of digestion methods

Complete decomposition is prerequisite for geological sample analysis using ICP-MS, and it is often the limiting factor of the data quality [4]. There are many digestion methods used in routine analysis of geological samples in different laboratories, including open vessel acid digestions, microwave dissolution, alkali fusion and high-pressure (bomb) digestions. The open vessel acid digestion on hotplate is successful for aphyric/glass volcanic rocks, but is incapable of digesting rock samples with refractory minerals, such as garnet, sphene, spinel, zircon, rutile and chromite [3,7]. Likewise, microwave dissolution with open or closed oven procedures do not have adequate energetics to digest refractory phases, resulting in incomplete recoveries of some elements [7,8]. Alkali fusion technique is effective to decompose resistant accessory minerals, but it causes high blank levels (i.e., flux impurities) and total dissolved solids (TDS). Besides, its high Si content can also cause complex isobaric interferences [3], plus causing significant instrumental drift during analysis due to silicate salt deposits in the interiors of the sample/skimmer cones [9]. In this case, the high-pressure digestion (bomb) method remains the method of choice, especially when applied to coarse grained granitic and metamorphic rocks [10–12].

However, the high-pressure digestion technique is not problem free. Despite its wide use, the problems involved and produced have not been well understood. On the basis of our repeated experiments on United States Geological Survey (USGS) rock reference standards, we demonstrate these problems below and offer our effective solutions.

### 3.2. Experiments, results and discussion

#### 3.2.1. Type of acids

Varying combination of strong acids is commonly used in the acid digestion of silicate materials, such as HF-$HClO_4$ [8,13,14], HF-$HNO_3$ [1,11,13,15], HF-HCl-$HClO_4$ [14], HF with aqua regia (1 $HNO_3$: 3 HCl) [16], HF-$H_2SO_4$ [4,8,13] or HF-HBr-$HNO_3$. More recently, a mixture of $NH_4F$-$HNO_3$ [3] or HF alone [12] is also used. It is suggested that the addition of $HClO_4$ is more effective to attack refractory minerals, such as those of the spinel group, and helps remove fluorides [7,17]. However, with issues such as safety and cost considered, very corrosive and explosive acids such as $HClO_4$ or $H_2SO_4$ should be avoided in geochemical laboratories [3,16]. Therefore, we conducted our experiments using HF-$HNO_3$ and HF-HCl-$HNO_3$.

#### 3.2.2. Digestion procedures

The USGS standard rock powders of W-2 (diabase), BCR-2 (basalt), BHVO-2 (basalt), AGV-2 (andesite), GSP-2 (granodiorite) were decomposed as follows (brief procedures were listed in Table 2): (1) Approximately 50 mg rock powder (grain size less than 200 mesh) was weighed in a 15 mL Teflon container, followed by the addition of 1 mL Lefort aqua regia (3 $HNO_3$:1 HCl) and 1 mL HF (Method A, B) or 1 mL Lefort aqua regia and 0.5 mL HF (Method C, D, E, F) or 1 mL $HNO_3$ and 0.5 mL HF (Method G); (2) the Teflon container was directly placed on a hotplate at 120 °C for 15 h (Method A) or inserted and sealed in a high-pressure metal jacket (Bomb) before placed in an oven at 190 °C for 8 h (Method F), 12 h (Method E) and 15 h (Method B, C, D, G); (3) After cooling, the Teflon container was opened and placed on a hotplate at 130 °C and evaporated to incipient dryness; (4) 1 mL $HNO_3$ was added and again evaporated to incipient dryness; (5) The sample was

**Table 2**
Brief sample digestion procedure for ICP-MS analyses.

| Method | First acid attack step | | | | | | Evaporate | | | Re-dissolution | | | |
|---|---|---|---|---|---|---|---|---|---|---|---|---|---|
| | T (°C) | Time (h) | $HNO_3$ (mL) | HCl (mL) | HF (mL) | Bomb / Hotplate | Time (h) | $HNO_3$ (mL) | T (°C) | Time (h) | $HNO_3$ (mL) | $H_2O$ (mL) | Bomb / Hotplate |
| (A) | 120 | 15 | 0.75 | 0.25 | 1 | Hotplate | ~3 | 1 | 120 | 12 | 1 | 4 | Hotplate |
| (B) | 190 | 15 | 0.75 | 0.25 | 1 | Bomb | ~3 | 1 | 190 | 2 | 1 | 4 | Bomb |
| (C) | 190 | 15 | 0.75 | 0.25 | 0.5 | Bomb | ~2.5 | 1 | 120 | 2 | 1 | 4 | Hotplate |
| (D) | 190 | 15 | 0.75 | 0.25 | 0.5 | Bomb | ~2.5 | 1 | 190 | 2 | 1 | 4 | Bomb |
| (E) | 190 | 12 | 0.75 | 0.25 | 0.5 | Bomb | ~2.5 | 1 | 190 | 2 | 1 | 4 | Bomb |
| (F) | 190 | 8 | 0.75 | 0.25 | 0.5 | Bomb | ~2.5 | 1 | 190 | 2 | 1 | 4 | Bomb |
| (G) | 190 | 15 | 1 | 0 | 0.5 | Bomb | ~2.5 | 1 | 190 | 2 | 1 | 4 | Bomb |

T (°C): temperature in Centigrade.

re-dissolved in the same container by adding 1 mL $HNO_3$ and 4 mL of ultra-pure water (Method A–G); (6) The container was then placed on a hotplate at 120 °C for 12 h (Method A) and 2 h (Method C) with the lid tightened, or inserted into bombs as above in the oven at 190 °C for 2 h (Method B, D–G); (7) The final solution was transferred to a polyethylene bottle and diluted to ~100 g of 2% v/v $HNO_3$.

### 3.2.3. Efficacies and drawbacks of high-pressure digestion technique

Our experiments confirm the results in the literature that the open vessel acid digestion (Method A) using hotplate at 120 °C (15 h) is effective for BCR-2 and AGV-2 (Fig. 1a), but is ineffective for GSP-2 with a poor recovery of Zr (~13%), Hf (~13%), Th (60%), U (80%) and most REEs (55%–76%) (Fig. 1a). In contrast, the high-pressure digestion method (Method D) shows highly effective in decomposing whatever aphyric/glass volcanic or granitic rocks or refractory phases (Fig. 1b, c). However, the outstanding drawback of the high pressure-temperature bomb digestion is the formation of insoluble fluoride complexes in which many trace elements are incorporated as we predict from our experiments (Fig. 1b, c).

In fact, the effect of fluorides in the high-T, high-P decompositions using bombs has been known for some time (c.f. [4] and reference therein). A quantitative evaluation by Takei et al. [15] further shows that fluoride formation is probably controlled by the chemical composition of the rock samples, in particular, the [(Mg + Ca)/Al] ratio of the sample. Accordingly, Takei et al. [15] developed a method to suppress the formation of fluorides and resulted in complete recovery of trace elements by adding Mg to the sample to produce [(Mg + Ca)/Al] > 1. It is suggested that the formation of such insoluble phases can be avoided if sample size is small and if the digestion mixture is ensured not to be completely dry during evaporation [3,9]. However, these methods to suppress fluoride formation are difficult to achieve and are not practical in routine analysis of geological samples. This is because (1) "pure reagent" of Mg solution is required, which inevitably demands excess time and cost; and we also must know the (Mg + Ca)/Al ratio in each unknown sample solution; (2) it is very difficult to control the extent of sample dryness, since this procedure is sample dependent [3]; (3) it is also not recommended for small sample size because few reference materials have their homogeneity tested at the milligram scale and real samples are not expected to be more homogeneous than reference materials [7]. Hence, the aforementioned remedy is not recommended.

It is important to note that despite the efficacy of the high-pressure bomb digestion technique in decomposing refractory phases, this technique also inevitably produces new and insoluble byproducts, which are suspected to be fluorides as discussed above. We predict that the byproducts may not be simple fluoride such as $AlF_3$ [12], but likely more than one complex. The fact that Sr is affected suggests the presence of fluoride such as $(Ca,Mg)F_2$,

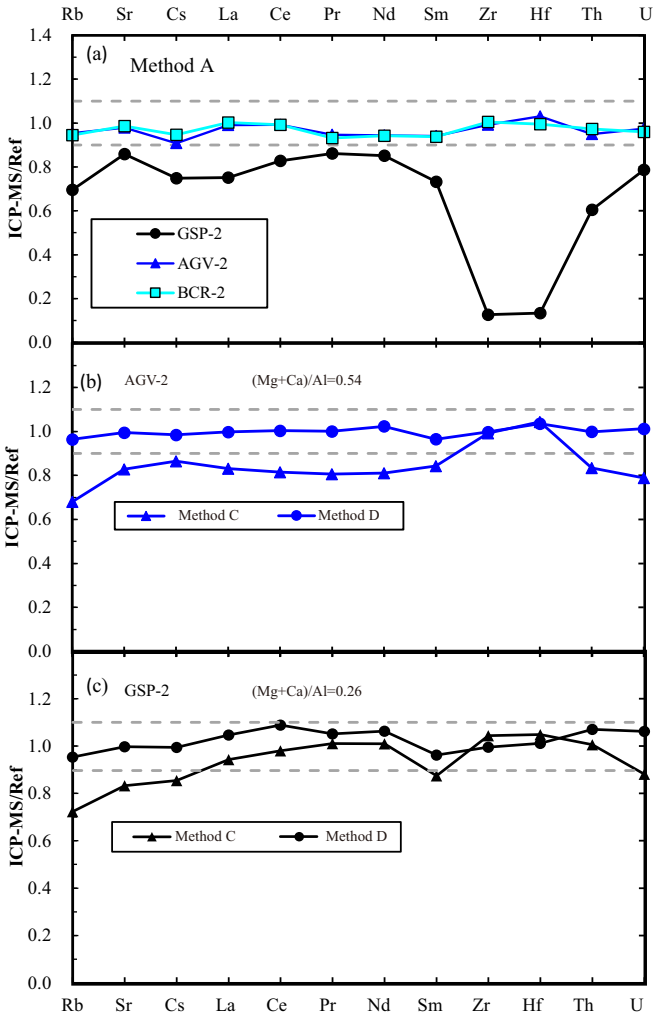


**Fig. 1.** (a) Recovery yields of selective trace elements for GSP-2, AGV-2 and BCR-2 using the method of open vessel acid digestions (Method A); (b–c) Recovery yields of these same elements for AGV-2 and GSP-2 using the high-pressure (bomb) digestion method with or without re-dissolution (Method D and C, respectively).

where Sr readily substitutes Ca. The effects on the trivalent REEs points to the presence of $Al^{3+}$ in the complex, which could be simple $AlF_3$ with Al substituted by REEs. However, we infer that other forms of fluoro-hydroxyl complexes are more likely, including the simple form of $Al(OH)_3$ or $Al(OH, F)_3$ because such complexes can absorb alkalis like K, Rb and Cs, which are also affected (Fig. 1b, c). The exact nature of such byproducts is to be further investigated, but our task at present is to decompose them.

Our experiments show that the byproducts formed during the high-pressure bomb digestion for 50 mg sample can be readily eliminated by re-dissolution under high pressure after evaporation. Fig. 1b and c demonstrate the data of re-dissolution using bomb at 190 °C for only 2 h (Method D). It should be noted that some laboratories may choose to digest more materials (e.g., ~100–200 mg), but at present we do not see the necessity of using excess materials for elemental analysis. Sample power inhomogeneity may be the potential need to use large amount of materials, but we emphasize that it is the responsibility of individual scientists to ensure complete sample homogeneity for analysis. Nevertheless, it is our interest to carry out this and other digestion experiments.

### 3.2.4. Effect of digestion time and type of acids

Fig. 2 illustrates the effect of digestion time on analytical results for Rb, La, Sr, Hf and Zr from GSP-2 at 190 °C using 1 mL Lefort aqua regia and 0.5 mL HF. The data show that Rb, La, Sr can be completely recovered by high-pressure digestion for less than 8 h, while 12 h are needed to completely recover Zr and Hf in GSP-2. To achieve rapid and cost-effective digestion, the effect of different acids was also investigated. As seen from Fig. 3, 0.5 mL HF in combination with 1 mL Lefort aqua regia show the same efficiency with 1 mL HF + 1 mL Lefort aqua regia and 1 mL $HNO_3$ + 0.5 mL HF for GSP-2 using bomb at 190 °C for 15 h. However, it is suggested that 18 h are needed for complete digestion of GSP-2 at above condition using 1 mL $HNO_3$ + 1 mL HF [12]. In this case, we choose to use the acid of 1 mL Lefort aqua regia + 0.5 mL HF (most effective) and 15 h (extra time) to ensure complete sample digestion in our routine sample analysis. Compared to widely used methods in some other laboratories (Fig. 4) [5,7,11,18–23], our less acid and less time method of sample digestion (<24 h vs. widely used >60 h) is very cost-effective.

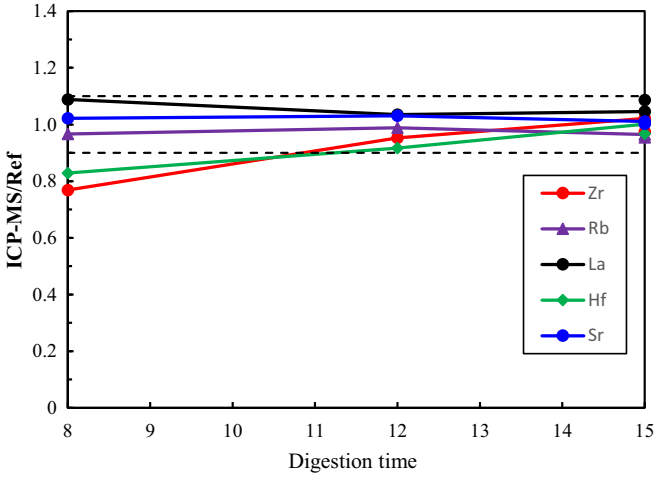


**Fig. 2.** Normalized concentrations of Rb, Sr, La, Zr and Hf (to reference values) for GSP-2 as a function of digestion time at 190 °C in a high pressure bomb. All digestions used acids of 1 mL Lefort aqua regia (3 $HNO_3$:1 HCl) and 0.5 mL HF.

## 4. Oxide and hydroxide interferences and corrections

### 4.1. A brief review of oxide and hydroxide interferences

The first major group of interferences associated with ICP-MS analysis are spectroscopic interferences, which are caused by atomic or molecular ions with the same mass-charge ratio ($m/z$) as the analyte element of interest. While these interferences caused by overlapping isotopes of different elements can be avoided by choosing alternative isotopes or elemental equations [24] in many cases, the formation of polyatomic ions, especially oxide and hydroxide in the plasma, are still practical problems that can give rise to inaccuracies during routine ICP-MS analysis [2]. The identification of oxide and hydroxide ions interferences have been discussed in many studies [2,24–26]. It has been well known that oxide and hydroxide ions levels are dependent on operating parameters such as plasma power, carrier gas flow rate, sample and skimmer orifice size [2,24–27]. As summarized by Evans and Giglio [26], there are various approaches towards reducing the oxide and hydroxide ions interference, including (1) alternative sample preparation methods, such as on-line separation, precipitation or solvent extraction; (2) alternative sample introduction methods, such as desolvation, laser ablation, and thermal vaporization; (3) alternative instrumentation, such as gas addition, dynamic reaction cells and high-resolution ICP-MS (HR-ICP-MS). These methods, however, are not applicable in routine multi-element analysis of geological samples using quadrupole ICP-MS (Q-ICP-MS) without desolvation systems.

Using mathematical corrections on raw data are suggested to be an alternative approach [2,24–26]. There are many types of corrections in the literature, it is therefore necessary to test existing

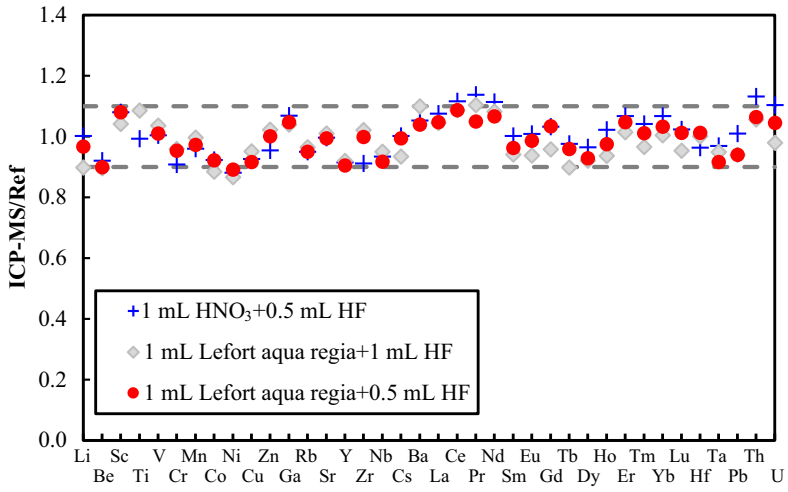


**Fig. 3.** Recoveries of thirty-eight elements (relative to reference values) for GSP-2 as a function of acids using bombs at 190 °C for 15 h. Digestion conditions: 1 mL Lefort aqua regia + 0.5 mL HF, 1 mL Lefort aqua regia + 1 mL HF and 1 mL $HNO_3$ + 0.5 mL HF.

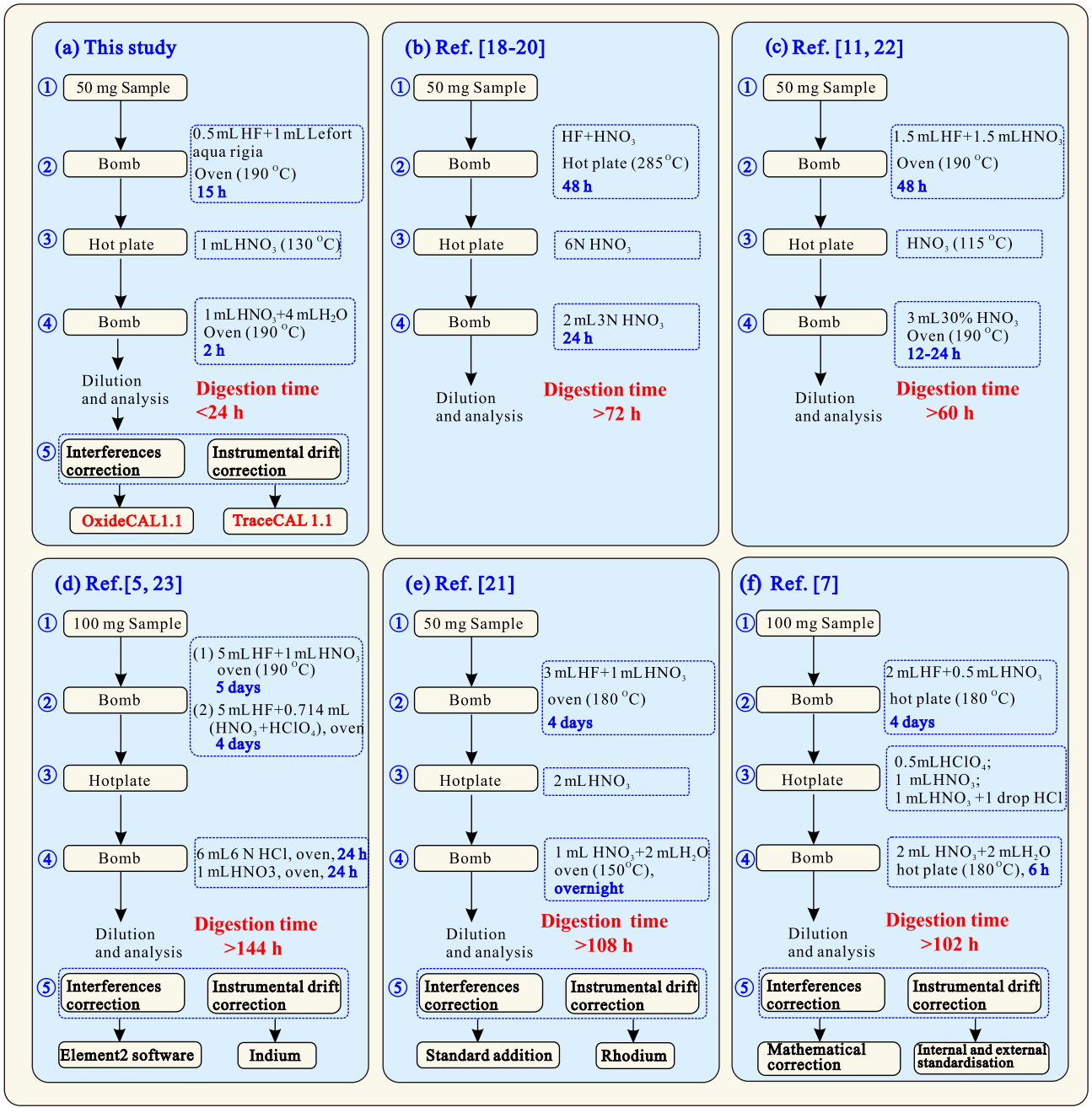


**Fig. 4.** Flow chart illustrating sample digestion (bomb procedures), interferences and instrumental drift corrections for analysis of trace element abundances in geological materials using ICP-MS in different laboratories from (a) this study, (b) Ref. [18–20], (c) Ref. [11], (d) Ref. [5], (e) Ref. [21], (f) Ref. [7]. The numbers in the left of each subplot are the procedures: ① weighing; ② first acid attack; ③ evaporation; ④ re-dissolution; ⑤ oxide, hydroxide and instrumental drift corrections.

methods and implement an effective and simple one to apply in routine multi-element analysis of geological materials using Q-ICP-MS.

### 4.2. Experiments and results

Quantification of oxide ($MO^+$) and hydroxide ($MOH^+$) ions is generally expressed as the oxide production ratio ($MO^+/M^+$) and hydroxide production ratio ($MOH^+/M^+$). For each element M, we first measured the intensities of $M^+$ ($m/z = m_i$), $MO^+$ ($m/z = m_i + 16$) and $MOH^+$ ($m/z = m_i + 17$) using mono-elemental solutions with different concentrations in the same run under standard conditions of the ICP-MS, and then calculated the $MO^+/M^+$ and $MOH^+/M^+$ ratios using a linear regression method. The above measurement was further repeated three times in different runs. The results can be found in Appendix Table A. Notably, the results for all these runs are similar to the observation of several authors [2,16,24], and two useful and important conclusions are:

(1) The $MO^+/M^+$ and $MOH^+/M^+$ ratios are not time-dependent or matrix-dependent, but remain constant in the same run (Table 3). As illustrated in Fig. S1, the intensities of $MO^+$ and $MOH^+$ increases linearly with the intensity of $M^+$ or the concentration of M. In fact, this is also manifested by the perfect coefficient of correlation ($R$) of the linear regression for most elements at three different runs (Fig. S1; Table 3).

(2) While the $MO^+/M^+$ and $MOH^+/M^+$ ratios vary between runs (Fig. 5), the $(MO^+/M^+)/(M'O^+/M'^+)$ and $(MOH^+/M^+)/(M'O^+/M'^+)$ ratios remain constant (Fig. 6; also see below).

**Table 3**
Oxide and hydroxide production rates (and their standard deviations, $\sigma$) used to calculate $k$(M/M′) and $k'$(M/M′) values.

| Element | Mass | Interference | First run | | Second run | | Third run | | First | Second | Third | Average | σ |
|---|---|---|---|---|---|---|---|---|---|---|---|---|---|
| | | | K | *R* | K | *R* | K | *R* | $k_{(MO/CeO)}$ or $k_{(MOH/CeO)}$ | | | | |
| Nd | 146 | $^{130}$BaO | 0.0002 | 0.7378 | 0.0004 | 0.9986 | 0.0003 | 0.9846 | | 0.0336 | 0.0312 | 0.0324 | 0.0017 |
| Sm | 147 | $^{130}$BaOH | 0.0010 | 0.9969 | 0.0009 | 0.9943 | 0.0012 | 0.9986 | 0.1026 | 0.0821 | 0.1187 | 0.1011 | 0.0183 |
| Sm | 150 | $^{134}$BaO | 0.0003 | 0.9999 | 0.0004 | 0.9999 | 0.0003 | 0.9998 | 0.0275 | 0.0344 | 0.0269 | 0.0296 | 0.0042 |
| Eu | 151 | $^{135}$BaO* | 0.0005 | 0.9998 | 0.0006 | 1.0000 | 0.0004 | 1.0000 | 0.0489 | 0.0521 | 0.0454 | 0.0488 | 0.0033 |
| Eu | 153 | $^{137}$BaO* | 0.0009 | 1.0000 | 0.0010 | 1.0000 | 0.0009 | 1.0000 | 0.0962 | 0.0865 | 0.0865 | 0.0897 | 0.0056 |
| Gd | 155 | $^{139}$LaO | 0.0069 | 1.0000 | 0.0088 | 1.0000 | 0.0074 | 1.0000 | 0.7352 | 0.7673 | 0.7488 | 0.7504 | 0.0161 |
| Gd | 156 | $^{140}$CeO | 0.0094 | 1.0000 | 0.0115 | 1.0000 | 0.0099 | 1.0000 | 1.0000 | 1.0000 | 1.0000 | 1.0000 | 0.0000 |
| Gd | 157 | $^{141}$PrO | 0.0105 | 1.0000 | 0.0115 | 1.0000 | 0.0109 | 1.0000 | 1.1140 | 0.9948 | 1.1008 | 1.0699 | 0.0653 |
| Tb | 159 | $^{143}$NdO* | 0.0106 | 1.0000 | 0.0122 | 1.0000 | 0.0107 | 1.0000 | 1.1286 | 1.0555 | 1.0877 | 1.0906 | 0.0366 |
| Dy | 163 | $^{147}$SmO | 0.0015 | 1.0000 | 0.0017 | 0.9998 | 0.0016 | 1.0000 | 0.1578 | 0.1496 | 0.1593 | 0.1556 | 0.0052 |
| Ho | 165 | $^{149}$SmO* | 0.0018 | 0.9994 | 0.0021 | 1.0000 | 0.0017 | 1.0000 | 0.1910 | 0.1797 | 0.1770 | 0.1826 | 0.0074 |
| Er | 167 | $^{151}$EuO | 0.0002 | 0.9902 | 0.0003 | 0.9994 | 0.0002 | 0.9986 | 0.0254 | 0.0245 | 0.0216 | 0.0238 | 0.0020 |
| Tm | 169 | $^{153}$EuO | 0.0003 | 1.0000 | 0.0003 | 0.9999 | 0.0002 | 0.9986 | 0.0299 | 0.0264 | 0.0224 | 0.0262 | 0.0037 |
| Yb | 172 | $^{156}$GdO | 0.0051 | 0.9996 | 0.0058 | 1.0000 | 0.0052 | 1.0000 | 0.5423 | 0.5052 | 0.5255 | 0.5244 | 0.0186 |
| Yb | 172 | $^{156}$DyO | 0.0044 | 0.9088 | 0.0042 | 0.9778 | 0.0056 | 1.0000 | | 0.3641 | 0.5700 | 0.4670 | 0.1456 |
| Yb | 173 | $^{157}$GdO* | 0.0055 | 0.9999 | 0.0060 | 1.0000 | 0.0056 | 1.0000 | 0.5847 | 0.5203 | 0.5710 | 0.5587 | 0.0339 |
| Lu | 175 | $^{159}$TbO | 0.0051 | 1.0000 | 0.0060 | 1.0000 | 0.0054 | 1.0000 | 0.5400 | 0.5219 | 0.5453 | 0.5357 | 0.0122 |
| Hf | 177 | $^{161}$DyO | 0.0027 | 1.0000 | 0.0031 | 1.0000 | 0.0027 | 1.0000 | 0.2902 | 0.2701 | 0.2778 | 0.2793 | 0.0102 |
| Hf | 178 | $^{162}$DyO | 0.0028 | 0.9999 | 0.0031 | 1.0000 | 0.0029 | 0.9999 | 0.3002 | 0.2713 | 0.2985 | 0.2900 | 0.0162 |
| Hf | 178 | $^{162}$ErO | 0.0018 | 0.7263 | 0.0046 | 0.9925 | 0.0041 | 0.6953 | | 0.3956 | | 0.3956 | |
| Ta | 181 | $^{165}$HoO | 0.0026 | 1.0000 | 0.0031 | 1.0000 | 0.0027 | 1.0000 | 0.2755 | 0.2681 | 0.2700 | 0.2712 | 0.0038 |
| Eu | 151 | $^{134}$BaOH* | 0.0015 | 0.9998 | 0.0020 | 1.0000 | 0.0015 | 1.0000 | 0.1615 | 0.1711 | 0.1512 | 0.1613 | 0.0100 |
| Eu | 153 | $^{136}$BaOH* | 0.0013 | 1.0000 | 0.0015 | 1.0000 | 0.0012 | 1.0000 | 0.1419 | 0.1276 | 0.1241 | 0.1312 | 0.0094 |
| Eu | 153 | $^{136}$CeOH | 0.0026 | 0.8934 | 0.0016 | 0.9998 | 0.0002 | 0.7464 | | 0.1400 | | 0.1400 | |
| Gd | 156 | $^{139}$LaOH | 0.0009 | 1.0000 | 0.0011 | 1.0000 | 0.0010 | 1.0000 | 0.1005 | 0.0982 | 0.1042 | 0.1010 | 0.0030 |
| Gd | 157 | $^{140}$CeOH | 0.0010 | 0.9999 | 0.0010 | 1.0000 | 0.0009 | 0.9997 | 0.1042 | 0.0907 | 0.0928 | 0.0959 | 0.0073 |
| Tb | 159 | $^{142}$CeOH | 0.0010 | 1.0000 | 0.0010 | 1.0000 | 0.0010 | 1.0000 | 0.1031 | 0.0886 | 0.0972 | 0.0963 | 0.0073 |
| Tb | 159 | $^{142}$NdOH* | 0.0048 | 1.0000 | 0.0054 | 1.0000 | 0.0049 | 1.0000 | 0.5063 | 0.4691 | 0.5008 | 0.4921 | 0.0201 |
| Dy | 163 | $^{146}$NdOH | 0.0006 | 0.9997 | 0.0006 | 0.9992 | 0.0004 | 0.9998 | 0.0636 | 0.0478 | 0.0452 | 0.0522 | 0.0099 |
| Ho | 165 | $^{148}$SmOH* | 0.0022 | 0.9995 | 0.0025 | 1.0000 | 0.0022 | 1.0000 | 0.2349 | 0.2200 | 0.2230 | 0.2260 | 0.0079 |
| Ho | 165 | $^{148}$NdOH | 0.0006 | 0.9947 | 0.0005 | 1.0000 | 0.0004 | 0.8491 | 0.0593 | 0.0416 | 0.0409 | 0.0473 | 0.0104 |
| Er | 167 | $^{150}$SmOH | 0.0003 | 0.9965 | 0.0003 | 0.9996 | 0.0003 | 0.9995 | 0.0288 | 0.0221 | 0.0256 | 0.0255 | 0.0034 |
| Er | 167 | $^{150}$NdOH | 0.0007 | 0.9945 | 0.0005 | 1.0000 | 0.0004 | 0.9986 | 0.0733 | 0.0409 | 0.0436 | 0.0526 | 0.0180 |
| Tm | 169 | $^{152}$SmOH | 0.0003 | 1.0000 | 0.0004 | 0.9990 | 0.0003 | 0.9949 | 0.0357 | 0.0313 | 0.0287 | 0.0319 | 0.0035 |
| Tm | 169 | $^{152}$GdOH | 0.0031 | 0.9999 | 0.0003 | 0.8576 | 0.0013 | 0.9722 | 0.3315 | | | 0.3315 | |
| Yb | 172 | $^{155}$GdOH | 0.0070 | 0.9996 | 0.0080 | 1.0000 | 0.0072 | 1.0000 | 0.7492 | 0.6899 | 0.7254 | 0.7215 | 0.0299 |
| Yb | 173 | $^{156}$GdOH* | 0.0042 | 1.0000 | 0.0046 | 1.0000 | 0.0044 | 1.0000 | 0.4423 | 0.3956 | 0.4450 | 0.4276 | 0.0278 |
| Yb | 173 | $^{156}$DyOH | 0.0004 | 0.2066 | 0.0028 | 0.9586 | 0.0002 | 0.3265 | | 0.2427 | | 0.2427 | |
| Lu | 175 | $^{158}$GdOH | 0.0005 | 0.9997 | 0.0006 | 1.0000 | 0.0005 | 0.9991 | 0.0570 | 0.0524 | 0.0517 | 0.0537 | 0.0029 |
| Lu | 175 | $^{158}$DyOH | 0.0016 | 0.6383 | 0.0026 | 0.9863 | -0.001 | 0.5657 | | 0.2248 | | 0.2248 | |
| Hf | 177 | $^{160}$GdOH | 0.0005 | 0.9996 | 0.0006 | 1.0000 | 0.0006 | 1.0000 | 0.0580 | 0.0523 | 0.0560 | 0.0554 | 0.0029 |
| Hf | 177 | $^{160}$DyOH | 0.0220 | 0.9999 | 0.0258 | 1.0000 | 0.0236 | 0.9999 | 2.3431 | 2.2365 | 2.3923 | 2.3240 | 0.0797 |
| Hf | 178 | $^{161}$DyOH | 0.0038 | 1.0000 | 0.0042 | 1.0000 | 0.0039 | 0.9999 | 0.4092 | 0.3658 | 0.3990 | 0.3913 | 0.0227 |
| Ta | 181 | $^{164}$DyOH | 0.0001 | 0.9776 | 0.0001 | 0.9994 | 0.0001 | 0.9998 | 0.0123 | 0.0114 | 0.0101 | 0.0112 | 0.0011 |
| Ta | 181 | $^{164}$ErOH | 0.0001 | 0.6905 | 0.0001 | 0.9869 | 0.0000 | 0.9385 | | 0.0074 | | 0.0074 | |

* The combination production of both oxidize and hydroxide (see text for details); K: the $MO^+/M^+$ and $MOH^+/M^+$ ratios calculated by linear regression; *R*: coefficient of correlation of the linear regression.

It should be noted that the second observation was consistent with the theoretical calculations by Shibata et al. [27]. That is, there was a linear correlation between the logarithmic term of $MO^+/M^+$ (log $MO^+/M^+$) values and dissociation energy, which mainly depends on plasma temperature and oxygen partial pressure. In combination with the theoretical calculations, these observations were further expressed by Dulski [14] as follows:

$$\frac{(MO^+/M^+)}{(M'O^+/M'^+)} = e^{(D^o_{MO}-D^o_{M'O})} = k_{(MO/M'O)}, \quad (1)$$

where $D^o_{MO}$ and $D^o_{M'O}$ is the dissociation energies of MO and M′O; $k_{(MO/M'O)}$ is the ratio of M and M′ oxide production ratios. By re-arranging the terms, we obtain Eq. (2):

$$(MO^+/M^+) = k_{(MO/M'O)} \times (M'O^+/M'^+), \quad (2)$$

### 4.3. Calibration strategy and a simple but useful Excel tool

From Eq. (2) above and our experimental data (Figs. 5 and 6), it is straightforward that any $MO^+$ and $MOH^+$ contribution can be calculated if one oxide production ratio ($M'O^+/M'^+$) was obtained during a run under standard conditions. Given the high concentration and high oxide production of Ce, we chose to measure the ratios of $^{140}CeO^+/^{140}Ce^+$ to correct for other oxide and hydroxide contributions. The general correcting equations have been documented in the literatures cited above, and are summarized below:

$$I^{m_i}_{LO^+} = I^{m_i-16}_{L^+,ori} \times (LO^+/L^+), \quad (3)$$

$$I^{m_i}_{NOH^+} = I^{m_i-17}_{N^+,ori} \times (NOH^+/N^+), \quad (4)$$

$$I^{m_i}_{M^+,cor} = I^{m_i}_{M^+,ori} - I^{m_i}_{LO^+} - I^{m_i}_{NOH^+}, \quad (5)$$

where $I^{m_i-16}_{L^+,ori}$ = Intensity of the ion $L^+$ signal at a given mass $m_i$–16, in cps; $I^{m_i}_{LO^+}$ = Intensity of oxide contribution ($LO^+$) signal of at mass $m_i$, in cps; $I^{m_i-17}_{N^+,ori}$ = Intensity of the ion $N^+$ signal at a given mass $m_i$–17, in cps; $I^{m_i}_{NOH^+}$ =Intensity of hydroxide contribution ($NOH^+$) signal of at mass $m_i$, in cps; $I^{m_i}_{M^+,ori}$ = Intensity of the total signal at a given mass $m_i$, in cps, before removal of the interferences; $I^{m_i}_{M^+,cor}$ = Intensity of

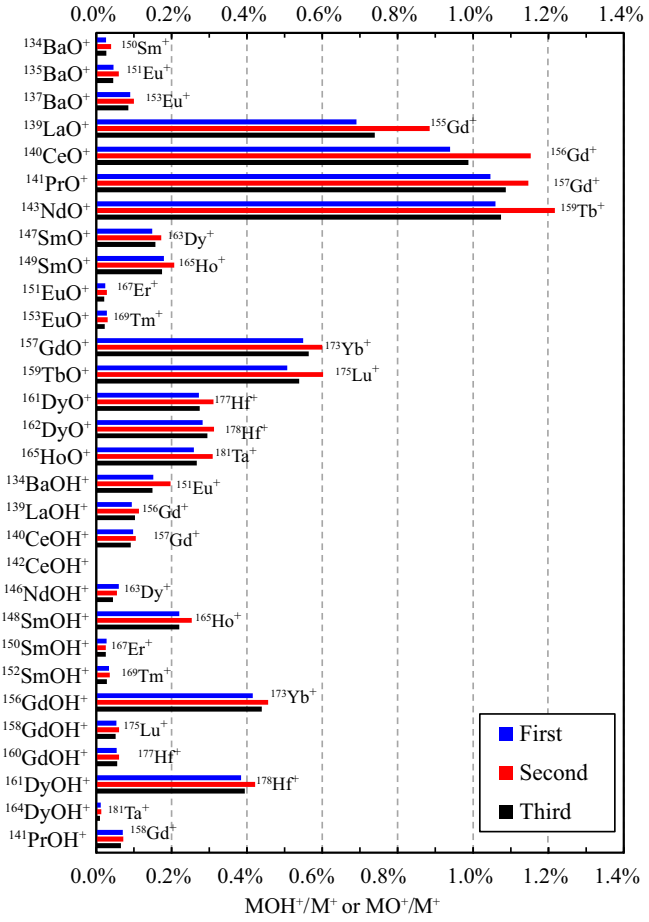


**Fig. 5.** Varying oxide ($MO^+/M^+$) and hydroxide ($MOH^+/M^+$) production of three individual runs.

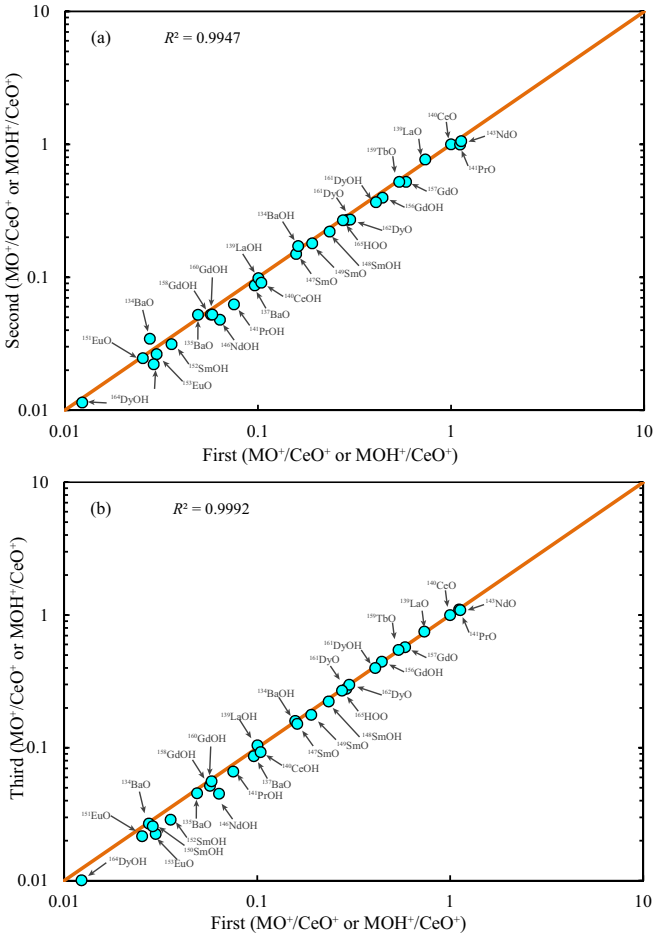


**Fig. 6.** The experimental results show constant ratios of $(MO^+/M^+)/(CeO^+/Ce^+)$ and $(MOH^+/M^+)/(CeO^+/Ce^+)$ at three individual runs. (a) First run vs. second run; (b) first run vs. third run.

the ion $M^+$ signal at a given mass $m_i$, in cps, after removal of the interferences.

Combining Eqs. (2) to (5) yields the following correcting Eq. (6):

$$I^{m_i}_{M^+,cor} = I^{m_i}_{M^+,ori} - I^{m_i-16}_{L^+,ori} \times k_{(LO/CeO)} \times (CeO^+/Ce^+) - I^{m_i-17}_{N^+,ori} \times k_{(NOH/CeO)} \times (CeO^+/Ce^+), \quad (6)$$

Some selected isotopes and their associated interference correction equations are given in Table 4. Theoretical correction equations are listed in the left column, however, it needs to be adjusted in practical use on the basis of the result of the oxide and hydroxide production using mono-elemental solutions (Table 3). Details on the correction equations used in our study are further explained as follows:

(1) To avoid over-correction, the oxide and hydroxide production ratios are used in the equations only when the correlation coefficient ($R$) of the linear regression is equal to or >0.95 for a given element for at least two runs. For example, in the case of $^{153}$Eu correction, the correlation coefficient of $^{136}CeOH^+/^{136}Ce^+$ is lower than 0.95 at the first run and third run, thus we adjust the theoretical correction equations to: $^{153}Eu^+ = {}^{153}M^+ - {}^{137}BaO^+ - {}^{136}BaOH^+$. In fact, the lower $R$ of oxides ($^{162}$ErO) and hydroxides ($^{136}$CeOH, $^{156}$DyOH, $^{158}$DyOH, $^{164}$ErOH) may attribute to their lower natural abundances (the natural abundance of $^{162}$Er, $^{136}$Ce, $^{156}$Dy, $^{158}$Dy, $^{164}$Er is 0.14%, 0.185%, 0.06%, 0.1%, 1.61%, respectively). It also means that they may be negligible in the correction in addition to their lower oxide and hydroxide production.

(2) It was sometimes impossible to distinguish oxide from hydroxide interferences; for example, in the case of Ba where $^{135}BaO^+$ and $^{134}BaOH^+$ interfere at $m/z = 151$. They are produced through:

$$I^{151}_{Eu^+} = I^{135}_{Ba^+} \times X_{135} + I^{134}_{Ba^+} \times X_{134}, \quad (7)$$

where $I^{151}_{Eu^+}$, $I^{135}_{Ba^+}$, $I^{134}_{Ba^+}$ is intensity of the ion $Eu^+$ signal at $m/z = 151$, and $Ba^+$ signal at $m/z = 135$ and 134, respectively, in cps; $X_{135}$ and $X_{134}$ is $^{135}BaO^+/^{135}Ba^+$ and $^{134}BaOH^+/^{134}Ba^+$, respectively.

Using the natural isotopic abundances of $^{134}$Ba (2.417%) and $^{135}$Ba (5.592%), we can obtain:

$$I^{134}_{Ba^+} = I^{135}_{Ba^+} \times \frac{134_{Ba}}{135_{Ba}} = I^{134}_{Ba^+} \times \frac{2.417\%}{5.592\%}, \quad (8)$$

Combining Eqs. (7) and (8) yields the following correcting Eq. (9):

$$I^{151}_{Eu^+} = I^{135}_{Ba^+} \times X_{135} + I^{135}_{Ba^+} \times (2.417\%/5.592\%) \times X_{134} = I^{135}_{Ba^+} \times X, \quad (9)$$

where $X = X_{135} + (2.417\%/5.592\%) \times X_{134}$.

It is then easily perceived that the coefficient X obtained from the linear regression method of $m/z = 151$ and 135 are the combination of both $^{135}BaO^+/^{135}Ba^+$ and $^{134}BaOH^+/^{134}Ba^+$. Thus, we adjust the theoretical correction equations to: $^{151}Eu^+ = {}^{151}M^+ - {}^{135}BaO^{+*}$, where $^{135}BaO^{+*}$ is the combination production of both $^{135}BaO^+$ and $^{134}BaOH^+$.

**Table 4**
Selected isotopes and their associated correction equations (*m*/*z*, oxide and hydroxide contributions).

| Element | Mass | Theoretical correction equations | Correction equations used in this study |
|---|---|---|---|
| Nd | 146 | $^{146}M^+$-$^{130}BaO^+$ | $^{146}M^+$ - $^{130}BaO^+$ |
| Sm | 147 | $^{147}M^+$-$^{130}BaOH^+$ | $^{147}M^+$-$^{130}BaOH^+$ |
| Eu | 151 | $^{151}M^+$-$^{135}BaO^+$-$^{134}BaOH^+$ | $^{151}M^+$-$^{135}BaO^{+*}$ |
| Eu | 153 | $^{153}M^+$-$^{137}BaO^+$-$^{136}BaOH^+$-$^{136}CeOH^+$ | $^{153}M^+$-$^{137}BaO^{+*}$ |
| Gd | 156 | $^{156}M^+$-$^{140}CeO^+$-$^{139}LaOH^+$-$^{156}Dy$ | $^{156}M^+$-$^{140}CeO^+$-$^{139}LaOH^+$-$^{156}Dy$ |
| Gd | 157 | $^{157}M^+$-$^{141}PrO^+$-$^{140}CeOH^+$ | $^{157}M^+$-$^{141}PrO^+$-$^{140}CeOH^+$ |
| Tb | 159 | $^{159}M^+$-$^{143}NdO^+$-$^{142}NdOH^+$-$^{142}CeOH^+$ | $^{159}M^+$-$^{143}NdO^{+*}$-$^{142}CeOH^+$ |
| Dy | 163 | $^{163}M^+$-$^{147}SmO^+$-$^{146}NdOH^+$ | $^{163}M^+$-$^{147}SmO^+$-$^{146}NdOH^+$ |
| Ho | 165 | $^{165}M^+$-$^{149}SmO^+$-$^{148}SmOH^+$-$^{148}NdOH^+$ | $^{165}M^+$-$^{149}SmO^{+*}$-$^{148}NdOH^+$ |
| Er | 167 | $^{167}M^+$-$^{151}EuO^+$-$^{150}NdOH^+$-$^{150}SmOH^+$ | $^{167}M^+$-$^{151}EuO^+$-$^{150}NdOH^+$-$^{150}SmOH^+$ |
| Tm | 169 | $^{169}M^+$-$^{153}EuO^+$-$^{152}SmOH^+$-$^{152}GdOH^+$ | $^{169}M^+$-$^{153}EuO^+$-$^{152}SmOH^+$ |
| Yb | 173 | $^{173}M^+$-$^{157}GdO^+$-$^{156}GdOH^+$-$^{156}DyOH^+$ | $^{173}M^+$-$^{157}GdO^{+*}$ |
| Lu | 175 | $^{175}M^+$-$^{159}TbO^+$-$^{158}GdOH^+$-$^{158}DyOH^+$ | $^{175}M^+$-$^{159}TbO^+$-$^{158}GdOH^+$ |
| Hf | 178 | $^{178}M^+$-$^{162}DyO^+$-$^{161}DyOH^+$-$^{162}ErO^+$ | $^{178}M^+$-$^{162}DyO^+$-$^{161}DyOH^+$ |
| Ta | 181 | $^{181}M^+$-$^{165}HoO^+$-$^{164}DyOH^+$-$^{164}ErOH^+$ | $^{181}M^+$-$^{165}HoO^+$-$^{164}DyOH^+$ |

* The combination production of both oxidize and hydroxide (see text for details).

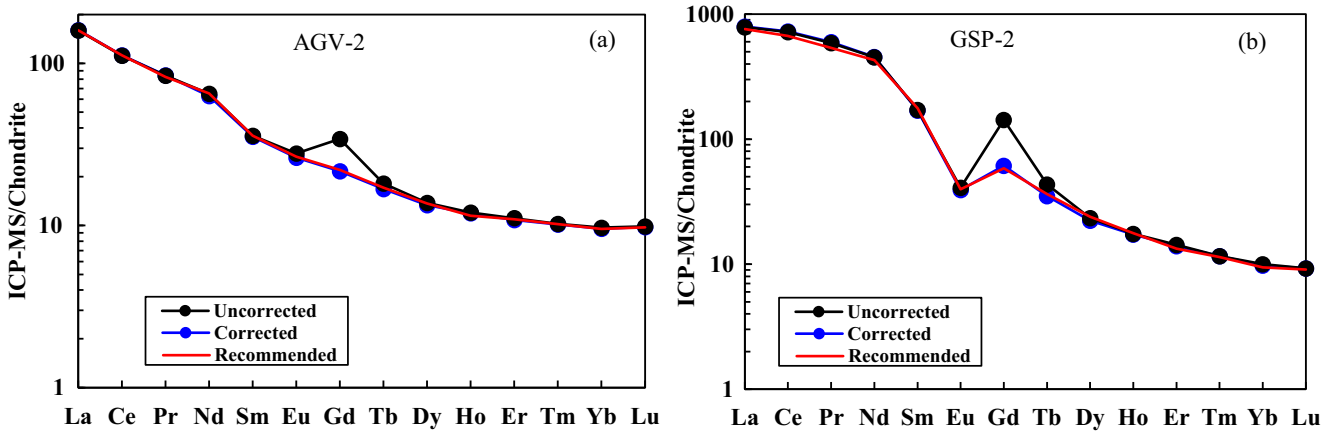


**Fig. 7.** (a–b) Examples of oxide and hydroxide correction using our procedure (given in the form of Excel). Chondrite-normalized REE patterns show the uncorrected, corrected and recommended values for (a) AGV-2 and (b) GSP-2. Chondrite REE values are from Sun and McDonough [38].

(3) It is sometimes not straightforward to correct for the interferences as the oxide or hydroxide isotope itself is interfered by other oxides or hydroxides. For instance, in the case of $^{173}Yb^+$ correction, the production of $^{156}GdOH^+$ should be subtracted using the intensity of $^{156}Gd^+$, however, $^{156}Gd^+$ itself is further interfered by $^{139}LaOH^+$ and $^{140}CeO^+$. In this case, it was necessary to deconvolute intensities using natural isotopic ratios.

On the basis of the experimental results and discussion above, we developed an Excel procedure to correct for the oxide and hydroxide interferences in routine analysis. As illustrated in Fig. 7, while this oxide and hydroxide correction procedure is an approximation, it is practical and effective. This Excel procedure and related manual can be download in Appendix Table B and Appendix Table D, respectively.

## 5. Instrumental drift during ICP-MS analysis and solutions

### *5.1. A brief review of solutions to instrumental drift during ICP-MS analysis in the literature*

Non-spectroscopic interferences are the second major group of interferences associated with ICP-MS. Our experience is consistent with the long known behavior that the instrumental drift during ICP-MS analysis is common and usually non-linear. The degree of drift differs from one mass to the next, and the direction of drift can change frequently [1,28]. Several methods are usually used to reduce the drift interference, single or multiple internal standards, standard additions, isotope dilution, external standard, and external calibration or a combine of several of the above [1,12,16,28,29]. Given the complex nature of instrumental drift as illustrated in Fig. 8, it would be difficult to monitor and correct for the drift by using single or even several internal standards [1,30]. It is considered that the method of standard additions (SA) or isotope dilution (ID) can avoid or minimize the drift, and improve the accuracy and precision [31,32]. However, the obvious drawbacks of their sophisticated, time-consuming and expensive procedures of both SA and ID methods have limited their application.

In this case, an interesting phenomenon that although the drift is virtually non-linear and the direction of drift can change frequently, the shape of the mass-time-intensity drift curve is always smooth, as previously observed [28] using VG Fisons PlasmaQuad ICP-MS for the analysis of Ba and REEs in geological samples (We note that the drift with time is smooth for a given isotope and systematic as a function of mass with the intensity going up or down and the so-called monotonic intensity decrease was not observed with the same instrument in Yaoling Niu's unpublished data available in 1994). On the basis of these observations, Cheatham et al. [28] developed an analytical procedure (called DCS, Drift correcting

**Table 5**
Analyses of USGS standards by ICPMS at the Institute of Oceanology, Chinese Academy of Sciences.

| | Isotope | Blank ($N$ = 10) | | W-2 ($N$ = 25, Digestion = 7) | | | | BHVO-2 ($N$ = 15, Digestion = 5) | | | | BCR-2 ($N$ = 15, Digestion = 7) | | | | AGV-2 ($N$ = 37, Digestion = 12) | | | | GSP-2 ($N$ = 23, Digestion = 7) | | | |
|---|---|---|---|---|---|---|---|---|---|---|---|---|---|---|---|---|---|---|---|---|---|---|---|
| | | AVE ppb | SD | AVG ppm | RSD % | RE % | Rec. ppm | AVG ppm | RSD % | RE % | Rec. ppm | AVG ppm | RSD % | RE % | Rec. ppm | AVG ppm | RSD % | RE % | Rec. ppm | AVG ppm | RSD % | RE % | Rec. ppm |
| Li | 7 | 0.017 | 0.021 | 8.40 | 3.0 | −9.7 | 9.30 | 4.16 | 5.5 | −13.2 | 4.80 | 8.54 | 4.1 | −5.1 | 9.00 | 9.94 | 3.7 | −9.7 | 11.0 | 34.8 | 3.5 | −3.2 | 36.0 |
| Be | 9 | 0.002 | 0.004 | 0.58 | 5.7 | −19.0 | 0.71 | 0.94 | 7.1 | −5.9 | 1.00 | 1.94 | 6.8 | −6.9 | 2.08 | 2.00 | 5.2 | −13.0 | 2.30 | 1.35 | 3.8 | −10.0 | 1.50 |
| Sc | 45 | 0.020 | 0.024 | 35.0 | 2.3 | −2.6 | 35.9 | 31.2 | 2.7 | −3.0 | 32.0 | 32.4 | 2.8 | −1.9 | 33.0 | 12.6 | 4.2 | −3.1 | 13.0 | 6.81 | 3.0 | 8.1 | 6.30 |
| Ti | 47 | 1.291 | 2.720 | 6434 | 1.9 | 1.2 | 6360 | 16600 | 2.2 | 1.5 | 16300 | 13598 | 2.6 | 0.7 | 13500 | 6152 | 2.9 | −2.3 | 6300 | 3981 | 2.8 | | |
| V | 51 | 0.128 | 0.064 | 272 | 1.7 | 1.6 | 268 | 326 | 2.3 | 2.5 | 317 | 424 | 2.7 | 2.0 | 416 | 119 | 2.7 | −2.6 | 122 | 53 | 2.7 | 1.0 | 52 |
| Cr | 53 | 0.408 | 0.200 | 86.2 | 2.1 | −7.3 | 93.0 | 287.2 | 3.3 | 2.3 | 280.0 | 14.8 | 3.5 | −17.8 | 18.0 | 15.2 | 3.4 | −5.1 | 16.0 | 19.1 | 3.1 | −4.6 | 20.0 |
| Mn | 55 | 0.154 | 0.205 | 1270 | 1.7 | −1.8 | 1294 | 1285 | 2.6 | −0.6 | 1290 | 1503 | 3.1 | −1.1 | 1520 | 748 | 2.8 | −2.9 | 770 | 312 | 2.8 | −2.6 | 320 |
| Co | 59 | 0.009 | 0.006 | 42.3 | 2.4 | −6.1 | 45.0 | 43.0 | 2.7 | −4.9 | 45.0 | 35.8 | 3.6 | −3.2 | 37.0 | 14.7 | 3.1 | −8.3 | 16.0 | 6.73 | 3.0 | −7.7 | 7.30 |
| Ni | 60 | 0.076 | 0.047 | 66.4 | 2.4 | −7.7 | 72.0 | 114.7 | 3.8 | −3.8 | 119.0 | 11.3 | 4.0 | −8.0 | 12.3[a] | 17.2 | 3.3 | −14.1 | 20.0 | 15.2 | 3.5 | −10.8 | 17.0 |
| Cu | 63 | 0.075 | 0.052 | 97.5 | 2.5 | −7.1 | 105.0 | 121.2 | 2.2 | −4.8 | 127.0 | 16.9 | 4.2 | −6.1 | 18.0[a] | 46.9 | 3.3 | −11.6 | 53.0 | 39.4 | 4.3 | −8.4 | 43.0 |
| Zn | 66 | 4.210 | 3.663 | 83.5 | 4.9 | 8.4 | 77.0 | 109.8 | 2.9 | 7.1 | 103.0 | 139.9 | 4.4 | 10.2 | 127.0 | 93.9 | 3.3 | 9.2 | 86.0 | 120 | 3.3 | 0.1 | 120 |
| Ga | 71 | 0.003 | 0.004 | 17.0 | 1.8 | −5.3 | 18.0 | 20.6 | 3.3 | −5.4 | 21.7 | 21.3 | 3.4 | −7.3 | 23.0 | 19.7 | 2.8 | −1.5 | 20.0 | 23.0 | 3.1 | 4.7 | 22.0 |
| Rb | 85 | 0.011 | 0.005 | 18.3 | 1.4 | −3.4 | 18.9 | 8.5 | 2.6 | −7.0 | 9.1 | 44.5 | 2.3 | −5.1 | 46.9 | 63.9 | 2.3 | −3.6 | 66.3 | 232.9 | 2.2 | −4.9 | 245.0 |
| Sr | 88 | 0.077 | 0.060 | 194 | 1.1 | −0.9 | 196 | 393 | 2.5 | −0.9 | 396 | 339 | 2.4 | −0.4 | 340 | 657 | 2.4 | −0.6 | 661 | 239 | 2.4 | −0.5 | 240 |
| Y | 89 | 0.003 | 0.004 | 20.1 | 1.7 | −8.5 | 22.0 | 24.2 | 2.5 | −7.0 | 26.0 | 33.4 | 2.5 | −9.7 | 37.0 | 18.3 | 2.5 | −3.7 | 19.0 | 25.3 | 2.3 | −9.5 | 28.0 |
| Zr | 90 | 0.052 | 0.035 | 90.4 | 1.8 | −1.8 | 92.0 | 167.9 | 2.4 | −2.6 | 172 | 183 | 2.8 | −0.3 | 184 | 230 | 2.5 | −0.1 | 230 | 549 | 3.9 | −0.1 | 550 |
| Nb | 93 | 0.004 | 0.003 | 6.69 | 2.0 | −10.9 | 7.50 | 16.86 | 2.6 | −7.1 | 18.1 | 11.36 | 2.5 | −9.9 | 12.6 | 12.8 | 2.5 | −11.7 | 14.5 | 24.8 | 2.4 | −8.3 | 27.0 |
| Cs | 133 | 0.002 | 0.002 | 0.87 | 1.5 | −5.0 | 0.92 | 0.10 | 3.7 | −2.7 | 0.10 | 1.14 | 2.7 | 3.6 | 1.10 | 1.16 | 2.3 | −0.2 | 1.16 | 1.19 | 2.3 | −0.6 | 1.20 |
| Ba | 137 | 0.042 | 0.034 | 168 | 2.3 | −2.1 | 172 | 129 | 3.6 | −1.4 | 131 | 689 | 2.8 | 1.7 | 677 | 1158 | 2.7 | 2.5 | 1130 | 1394 | 2.7 | 4.0 | 1340 |
| La | 139 | 0.003 | 0.003 | 10.3 | 1.8 | −4.2 | 10.8 | 15.0 | 2.4 | −1.2 | 15.2 | 25.0 | 2.4 | 0.5 | 24.9 | 38.0 | 2.5 | 0.4 | 37.9 | 189 | 2.0 | 4.8 | 180 |
| Ce | 140 | 0.004 | 0.007 | 22.6 | 1.6 | −3.6 | 23.4 | 36.8 | 2.2 | −1.8 | 37.5 | 52.3 | 2.1 | −1.1 | 52.9 | 68.7 | 2.2 | 0.1 | 68.6 | 446 | 1.9 | 8.7 | 410 |
| Pr | 141 | 0.001 | 0.001 | 2.92 | 1.3 | −2.8 | 3.00 | 5.17 | 2.1 | −3.4 | 5.35 | 6.69 | 1.9 | −0.2 | 6.70 | 8.02 | 2.3 | 2.3 | 7.84 | 56.72 | 2.0 | −3.2 | 58.6[a] |
| Nd | 146 | 0.003 | 0.004 | 12.3 | 3.5 | −5.4 | 13.0 | 23.1 | 3.9 | −5.6 | 24.5 | 27.5 | 3.7 | −4.3 | 28.7 | 29.4 | 4.1 | −3.5 | 30.5 | 213 | 2.0 | 6.6 | 200 |
| Sm | 147 | 0.001 | 0.001 | 3.19 | 1.9 | −3.3 | 3.30 | 5.93 | 2.2 | −2.5 | 6.07 | 6.43 | 2.4 | −2.3 | 6.58 | 5.41 | 2.4 | −1.5 | 5.49 | 26.01 | 2.2 | −3.7 | 27.00 |
| Eu | 151 | 0.001 | 0.001 | 1.07 | 2.2 | −0.7 | 1.08 | 2.02 | 2.4 | −2.4 | 2.07 | 1.94 | 2.1 | −1.2 | 1.96 | 1.52 | 2.1 | −1.1 | 1.54 | 2.27 | 2.2 | −1.3 | 2.30 |
| Gd | 157 | 0.001 | 0.001 | 3.56 | 4.4 | −2.7 | 3.66 | 5.94 | 4.0 | −4.3 | 6.24 | 6.55 | 2.9 | −3.0 | 6.75 | 4.45 | 3.1 | −1.7 | 4.52 | 12.41 | 4.9 | 3.4 | 12.00 |
| Tb | 159 | 0.001 | 0.001 | 0.61 | 1.8 | −1.6 | 0.62 | 0.92 | 2.4 | 0.1 | 0.92 | 1.05 | 2.7 | −2.2 | 1.07 | 0.63 | 2.9 | −1.9 | 0.64 | 1.31 | 2.7 | −4.0 | 1.36 |
| Dy | 163 | 0.001 | 0.001 | 3.74 | 2.0 | −1.4 | 3.79 | 5.08 | 3.4 | −4.3 | 5.31 | 6.19 | 3.5 | −3.5 | 6.41 | 3.40 | 3.0 | −2.1 | 3.47 | 5.66 | 2.8 | −7.1 | 6.10 |
| Ho | 165 | 0.001 | 0.001 | 0.80 | 1.8 | 0.7 | 0.79 | 0.98 | 2.4 | 0.0 | 0.98 | 1.31 | 2.4 | 2.0 | 1.28 | 0.67 | 2.4 | 3.6 | 0.65 | 0.98 | 2.2 | −2.5 | 1.00 |
| Er | 167 | 0.001 | 0.001 | 2.19 | 2.2 | −1.5 | 2.22 | 2.46 | 3.6 | −3.0 | 2.54 | 3.61 | 2.4 | −1.5 | 3.66 | 1.79 | 3.2 | −1.1 | 1.81 | 2.30 | 2.2 | −2.8 | 2.37 |
| Tm | 169 | 0.000 | 0.001 | 0.32 | 1.4 | −2.8 | 0.33 | 0.33 | 2.8 | 0.0 | 0.33 | 0.53 | 2.9 | −2.7 | 0.54 | 0.26 | 2.9 | −0.5 | 0.26 | 0.29 | 2.9 | 1.2 | 0.29 |
| Yb | 173 | 0.001 | 0.001 | 2.05 | 2.1 | 0.1 | 2.05 | 1.96 | 2.2 | −2.6 | 2.00 | 3.35 | 2.3 | −1.0 | 3.38 | 1.63 | 2.9 | 0.3 | 1.62 | 1.65 | 2.9 | 3.3 | 1.60 |
| Lu | 175 | 0.000 | 0.001 | 0.31 | 2.3 | −1.6 | 0.31 | 0.27 | 2.4 | −1.1 | 0.27 | 0.50 | 3.0 | −0.4 | 0.50 | 0.25 | 3.2 | 0.8 | 0.25 | 0.23 | 3.1 | 1.3 | 0.23 |
| Hf | 178 | 0.002 | 0.001 | 2.44 | 2.7 | −0.3 | 2.45 | 4.35 | 3.2 | −0.3 | 4.36 | 4.86 | 2.5 | −0.9 | 4.90 | 5.18 | 2.6 | 3.5 | 5.00 | 14.2 | 3.6 | 1.3 | 14.0 |
| Ta | 181 | 0.001 | 0.001 | 0.44 | 2.8 | −6.2 | 0.47 | 1.09 | 2.3 | −4.3 | 1.14 | 0.73 | 1.5 | −1.0 | 0.74 | 0.80 | 1.8 | −8.0 | 0.87 | 0.82 | 2.0 | −8.3 | 0.90 |
| Pb | 208 | 0.042 | 0.029 | 7.20 | 3.4 | −6.4 | 7.70 | 1.46 | 5.9 | −6.7 | 1.60 | 9.40 | 4.8 | −14.6 | 11.0 | 12.3 | 3.4 | −6.8 | 13.2 | 39.5 | 2.7 | −6.0 | 42.0 |
| Th | 232 | 0.001 | 0.001 | 2.12 | 1.7 | −2.1 | 2.17 | 1.18 | 2.2 | −3.4 | 1.22 | 5.78 | 1.5 | 1.5 | 5.70 | 6.09 | 1.9 | −0.1 | 6.10 | 112 | 1.9 | 6.4 | 105 |
| U | 238 | 0.001 | 0.001 | 0.49 | 2.1 | −3.3 | 0.51 | 0.41 | 2.0 | 1.3 | 0.40 | 1.66 | 1.8 | -2.1 | 1.69 | 1.88 | 1.9 | 1.2 | 1.86 | 2.51 | 2.0 | 4.6 | 2.40 |

$N$: number of analyses; AVG: average of measured value; Rec.: recommended value; RSD: relative standard deviation; RE: relative error between measured and recommended values. Recommended values are from GemReM (http://minerals.cr.usgs.gov/geo_chem_stand/) and Govindaraju (1994). [a]Ni, Cu in BCR-2 and Pr in GSP-2 are exceptions, which are taken from Ref. [12].

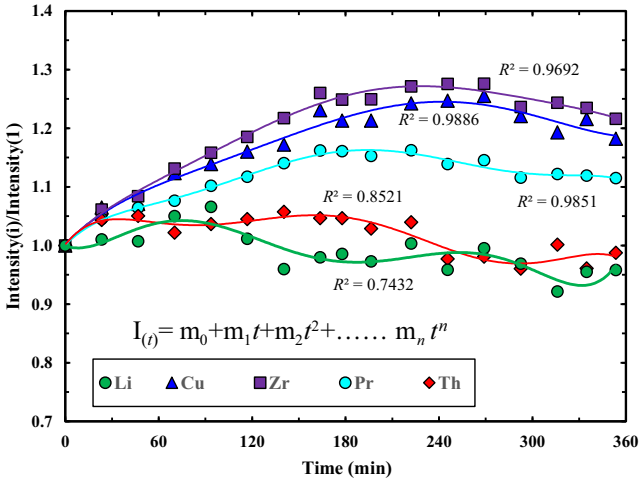


**Fig. 8.** Curvilinear instrumental drift for representative elements of low to high mass as a function of time.

solutions) and an off-line data reduction algorithm to correct for the drift. In this technique, they fit a polynomial curve, generated by repeated measurement of a "drift correction" standard after every few unknown samples, to each isotope analyzed and apply a correction based on this curve to the measured intensity of the respective isotope. This procedure was successful with a significant improvement in analytical accuracy and precision. Liu et al. [33] further developed this procedure to correct for drift in the LA-ICP-MS technique by normalizing the sum of all the major element oxides to 100 wt.%.

While the new generations of ICP-MS such as Agilent 7900 that we use have been significantly improved over the past 20 years, the instrumental drift remains an unresolved problem with drift patterns (Fig. 8) statistically and randomly similar to what were observed as before [28]. Hence, the concept of drift correction described in [28] is still applicable. Given the DCS procedure for Macintosh Excel macro is no longer available, we developed a new procedure and software.

### 5.2. Calibration strategy and an update Microsoft Excel VBA procedure

In this section, we describe a new procedure for drift correction developed in Microsoft Excel Visual Basic for Applications (VBA) following the concept of [28]. We aim to provide an update and free tool, which is easy to use, available to all users to correct for the drift during ICP-MS analysis. The calibration strategy is based on the following steps and equations.

Step 1: Fitting a mass-time-intensity drift curve for each analyzed element by repeated measurement of a QC (quality control) solution, as shown by Eq. (10)

$$\mathrm{Iqc}^{\mathrm{i}}_{(t)} = \mathrm{m}_0 + \mathrm{m}_1 t + \mathrm{m}_2 t^2 + \ldots + \mathrm{m}_j t^j, \quad (10)$$

where $t$ = the time interval between the first QC and the following QC (or sample), $\mathrm{Iqc}^{\mathrm{i}}_{(t)}$ = intensity of element of interest i in the QC at time $t$, and $\mathrm{m}_0$, $\mathrm{m}_1$ and $\mathrm{m}_j$ are the coefficients of the polynomial.

Step 2: Calculating the intensity drift factor for each analyzed element at given time.

It should be noted that the first QC is measured after the standard solutions, which is assumed to have no drift. This assumption and Eq. (10) imply that the intensity drift of each analyzed element at any time of an unknown sample analysis can be obtained, e.g. Eq. (11):

$$k^{\mathrm{i}}_{(t)} = \mathrm{Iqc}^{\mathrm{i}}_{(t)} / \mathrm{Iqc}^{\mathrm{i}}_{(1)}, \quad (11)$$

where $\mathrm{Iqc}^{\mathrm{i}}_{(1)}$ = the intensity of analyzed element i in the first QC, $k^{\mathrm{i}}_{(t)}$ = the intensity drift factor of element i at time $t$.

Step 3: Calibrating the drift

Combining Eqs. (10) and (11) yields the following correcting Eqs. (12) and (13):

$$\mathrm{Isam}^{\mathrm{i}}_{(t)}\mathrm{corr} = \mathrm{Isam}^{\mathrm{i}}_{(t)} / k^{\mathrm{i}}_{(t)}, \quad (12)$$

$$\mathrm{Isam}^{\mathrm{i}}_{(t)}\mathrm{corr} = \mathrm{Isam}^{\mathrm{i}}_{(t)} \times \mathrm{Iqc}^{\mathrm{i}}_{(1)} / (\mathrm{m}_0 + \mathrm{m}_1 t + \mathrm{m}_2 t^2 + \ldots + \mathrm{m}_j t^j), \quad (13)$$

where $\mathrm{Isam}^{\mathrm{i}}_{(t)}$ = original intensity of analyzed element i in the sample at time $t$, and $\mathrm{Isam}^{\mathrm{i}}_{(t)}\mathrm{corr}$ = the corrected intensity of element i in the sample at time $t$.

Following the above steps and strategy, we developed an off-line Microsoft Excel VBA procedure (TraceCAL) that completely automates all calculations to correct for the drift during ICP-MS analysis. The VBA procedure TraceCAL 1.1 and relevant Microsoft Excel VBA codes and manuals can be downloaded in Appendix Table C and Appendix D, respectively. It should be noted that the current version of TraceCAL 1.1 was designed to correct for the

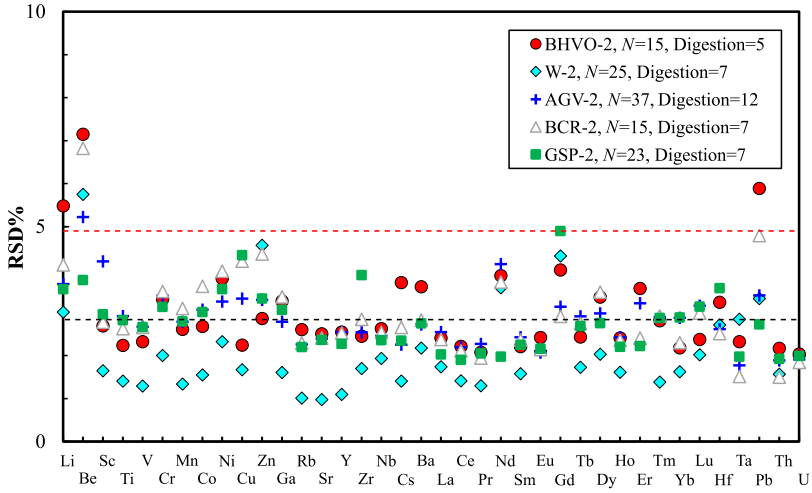


**Fig. 9.** The relative standard deviation (RSD % = 1$\sigma$ × 100/average) from the determined average values of five USGS standards for elements given using different individual digestions and analyses. The dash black and red line show RSD% = 3% and 5%, respectively.

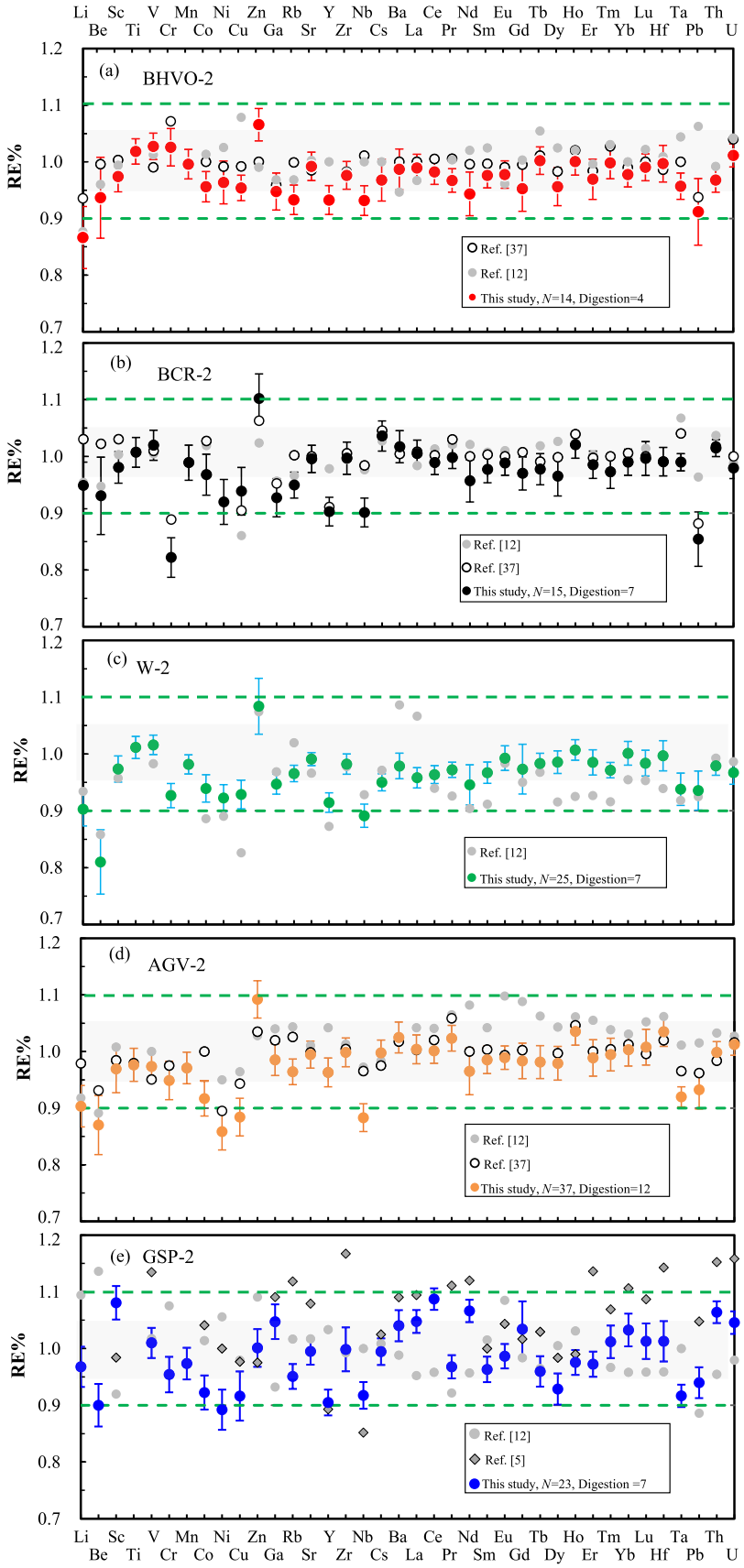


**Fig. 10.** (a–e) Trace element abundances normalized to the recommended values of Govindaraju [34] and GeoReM (http://georem.mpch-mainz.gwdg.de/) for (a) BHVO-2, (b) BCR-2, (c) W-2, (d) AGV-2, (e) GSP-2. The recent literature data [5,12,37] are also plotted for comparison. The dash green lines show the discrepancies of 10% between the determined values and the recommended values, and the shade area are within 5%.

drift using concentration of analyzed elements rather than intensity, because of their linear correlation. The update version, which combines oxide, hydroxide and drift corrections, are to be made available soon. In addition, on the basis of the long-term practice in our lab, we recommend each run of samples should be within 4 h, beyond which oxide, hydroxide and drift corrections may become ineffective.

## 6. Analysis of reference materials

Table 5a–b shows results for five USGS rock reference standards (BHVO-2, W-2, BCR-2, AGV-2, GSP-2) analyzed in our laboratory using the methods described above. The values for BHVO-2, W-2, BCR-2, AGV-2, GSP-2 are averages of many analyses of individual digestions/solutions (Table 5a–b). The data give precisions generally better than 5% for most elements (Fig. 9). Accuracy, as indicated by relative difference (RE) between measured and recommended values of Govindaraju [34] and GeoReM (http://georem.mpch-mainz.gwdg.de/) is better than 8%, with many elements agreeing to within 5% of the reference values. Exceptions are: (1) Li (4.16 ppm) in BHVO-2, which is about 13.2% lower than the reference value (4.8 ppm); (2) Li (9.94 ppm), Be (2 ppm), Cr (15.2 ppm), Ni (17.2 ppm), Co (14.7 ppm), and Cu (46.9 ppm) in AGV-2, which are about 10% lower than the reference values; (3) Li (8.4 ppm) and Be (0.58 ppm) in W-2, which are 9.7% and 19% lower than the reference values, respectively; (4) Cr (14.8 ppm), and Pb (9.4 ppm) in BCR-2 are about 15% lower than the reference values; (5) Be (1.35 ppm), Ni (15.2 ppm), Cu (39.4 ppm), Ta (0.82 ppm) in GSP-2 are about 10% lower than the reference values, and Ce (446 ppm) is 8.7% higher than the reference values. These discrepancies between our analyses and reference values, however, are in good agreement with the recent published data (Fig. 10) [12,23,35–37]. It is also notable that the Nb value we obtained for all the five USGS standards are about 9% lower than the reference values, which may be due to inaccurate Nb concentration in our Multi-element Calibration Standard solutions. Accordingly, the Nb concentration measured in our samples can be corrected if proven to be necessary.

## 7. Conclusions

(1) While the high-pressure digestion technique is effective in decomposing refractory phases, it also introduces insoluble byproducts, whose exact form or forms are yet to be further investigated, but they are most likely fluorides and fluorohydroxyl complexes, including (but not limited to) (Ca,Mg)$F_2$, $Al(OH,F)_3$. Nevertheless, these byproducts can be easily eliminated by re-dissolution using bombs at 190 °C for only 2 h for 50 mg sample. This is a very cost-effective advancement in ICP-MS analysis of geological materials.

(2) We have shown that, although oxide ($MO^+/M^+$) and hydroxide productions ($MOH^+/M^+$) are variable between analytical runs, the $(MO^+/M^+)/(CeO^+/Ce^+)$ and $(MOH^+/M^+)/(CeO^+/Ce^+)$ ratios remain constant. With this observation and by determining oxide and hydroxide production using mono-element solutions, we developed an off-line procedure for oxide and hydroxide corrections from the raw data by using a set of equations.

(3) The instrumental drift during ICP-MS analysis observed in early days [28] remains a major analytical problem with drift patterns as a function of time in an analytical run and systematics as a function of mass randomly and statistically the same and unresolved. We have thus, following the concept of [28], designed an off-line procedure for correcting instrumental drift without the need of internal standards.

(4) On the basis of many purpose-designed experiments for sample digestion/dissolution, oxide/hydroxide correction and drift correction, we established a simple and cost-effective set of procedures for rapid and precise analysis of trace element abundances in geological materials with ICP-MS. This represents an analytical innovation and advancement, and can be readily applied in other ICP-MS laboratories.

## Conflict of interest

The authors declare that they have no conflict of interest.

## Acknowledgments

This work was supported by National Natural Science Foundation of China (41130314 and 41630968), Chinese Academy of Sciences Innovation Grant (Y42217101L), Qingdao National Laboratory for Marine Science and Technology (2015ASKJ03) and Marine Geological Process and Environment (U1606401).

## Appendix A. Supplementary data

Supplementary data associated with this article can be found, in the online version, at http://dx.doi.org/10.1016/j.scib.2017.01.004.

## References

[1] Eggins SM, Woodhead JD, Kinsley LPJ, et al. A simple method for the precise determination of ⩾40 trace elements in geological samples by ICPMS using enriched isotope internal standardisation. Chem Geol 1997;134:311–26.
[2] Aries S, Valladon M, Polvé M, et al. A routine method for oxide and hydroxide interference corrections in icp-ms chemical analysis of environmental and geological samples. Geostand Geoanal Res 2000;24:19–31.
[3] Hu Z, Gao S, Liu Y, et al. $NH_4F$ assisted high pressure digestion of geological samples for multi-element analysis by ICP-MS. J Anal At Spectrom 2010;25:408–13.
[4] Chao TT, Sanzolone RF. Decomposition techniques. J Geochem Explor 1992;44:65–106.
[5] Pretorius W, Weis D, Williams G, et al. Complete trace elemental characterisation of granitoid (USGS G-2, GSP-2) reference materials by high resolution inductively coupled plasma-mass spectrometry. Geostand Geoanal Res 2006;30:39–54.
[6] Agatemor C, Beauchemin D. Matrix effects in inductively coupled plasma mass spectrometry: a review. Anal Chim Acta 2011;706:66–83.
[7] Cotta AJB, Enzweiler J. Classical and new procedures of whole rock dissolution for trace element determination by ICP-MS. Geostand Geoanal Res 2012;36:27–50.
[8] Totland M, Jarvis I, Jarvis KE. An assessment of dissolution techniques for the analysis. Chem Geol 1992;95:35–62.
[9] Navarro MS, Andrade S, Ulbrich H, et al. The direct determination of rare earth elements in basaltic and related rocks using ICP-MS: testing the efficiency of microwave oven sample decomposition procedures. Geostand Geoanal Res 2008;32:167–80.
[10] Rudnick RL, Gao S, W-l Ling, et al. Petrology and geochemistry of spinel peridotite xenoliths from Hannuoba and Qixia, North China Craton. Lithos 2004;77:609–37.
[11] Liu Y, Zong K, Kelemen PB, et al. Geochemistry and magmatic history of eclogites and ultramafic rocks from the Chinese continental scientific drill hole: subduction and ultrahigh-pressure metamorphism of lower crustal cumulates. Chem Geol 2008;247:133–53.
[12] Zhang W, Hu Z, Liu Y, et al. Reassessment of $HF/HNO_3$ decomposition capability in the high-pressure digestion of felsic rocks for multi-element determination by ICP-MS. Geostand Geoanal Res 2012;36:271–89.
[13] Yu Z, Philip R, Peter MG. An evaluation of methods for the chemical decomposition of geological materials for trace element determination using ICP-MS. Geostand Geoanal Res 2001;25:199–217.
[14] Dulski P. Reference materials for geochemical studies: new analytical data by ICP-MS and critical discussion of reference values. Geostand Geoanal Res 2001;25:87–125.
[15] Takei H, Yokoyama T, Makishima A, et al. Formation and suppression of AlF3 during HF digestion of rock samples in Teflon bomb for precise trace element analyses by ICP-MS and ID-TIMS. Proceed Jpn Acad, Ser B 2001;77:13–7.
[16] Niu Y, Batiza R. Trace element evidence from seamounts for recycled oceanic crust in the Eastern Pacific mantle. Earth Planet Sci Lett 1997;148:471–83.
[17] Yokoyama T, Makishima A, Nakamura E. Evaluation of the coprecipitation of incompatible trace elements with fluoride during silicate rock dissolution by acid digestion. Chem Geol 1999;157:175–87.

[18] Song S, Wang M-M, Xu X, et al. Ophiolites in the Xing'an-Inner Mongolia accretionary belt of the CAOB: implications for two cycles of seafloor spreading and accretionary orogenic events. Tectonics 2015;34:2221–48.
[19] Guo P, Niu Y, Ye L, et al. Lithosphere thinning beneath west North China Craton: evidence from geochemical and Sr–Nd–Hf isotope compositions of Jining basalts. Lithos 2014;202–203:37–54.
[20] Chen S, Niu Y, Sun W, et al. On the origin of mafic magmatic enclaves (MMEs) in syn-collisional granitoids: evidence from the Baojishan pluton in the North Qilian Orogen, China. Mineral Petrol 2015:1–20.
[21] Gaschnig RM, Rudnick RL, McDonough WF. Determination of Ga, Ge, Mo, Ag, Cd, In, Sn, Sb, W, Tl and Bi in USGS whole-rock reference materials by standard addition ICP-MS. Geostand Geoanal Res 2015;39:371–9.
[22] He D, Liu Y, Tong X, et al. Multiple exsolutions in a rare clinopyroxene megacryst from the Hannuoba basalt, North China: implications for subducted slab-related crustal thickening and recycling. Lithos 2013;177:136–47.
[23] Carpentier M, Weis D, Chauvel C. Large U loss during weathering of upper continental crust: the sedimentary record. Chem Geol 2013;340:91–104.
[24] Dulski P. Interferences of oxide, hydroxide and chloride analyte species in the determination of rare earth elements in geological samples by inductively coupled plasma-mass spectrometry. Fresenius J Anal Chem 1994;350:194–203.
[25] Ketterer ME, Biddle DA. Multivariate calibration in inductively coupled plasma mass spectrometry. 2. Effect of changes in abundances of interfering polyatomic ions. Anal Chem 1992;64:1819–23.
[26] Evans EH, Giglio JJ. Interferences in inductively coupled plasma mass spectrometry. A review. J Anal At Spectrom 1993;8:1–18.
[27] Shibata N, Fudagawa N, Kubota M. Oxide formation in electrothermal vaporization inductively coupled plasma mass spectrometry. Spectrochim Acta Part B At Spectrosc 1993;48:1127–37.
[28] Cheatham MM, Sangrey WF, White WM. Sources of error in external calibration ICP-MS analysis of geological samples and an improved non-linear drift correction procedure. Spectrochim Acta Part B At Spectrosc 1993;48:487–506.
[29] Thompson JJ, Houk RS. A study of internal standardization in inductively coupled plasma-mass spectrometry. Appl Spectrosc 1987;41:801–6.
[30] Al-Ammar AS. Simultaneous correction for drift and non-spectroscopic matrix effect in the measurement of geological samples by inductively coupled plasma-mass spectrometry using common analyte internal standardization chemometric technique. Spectrochim Acta Part B At Spectrosc 2003;58:1391–401.
[31] Xie Q, Jain J, Sun M, et al. ICP-MS analysis of basalt BIR-1 for trace elements. Geostand Geoanal Res 2007;18:53–63.
[32] Longerich HP, Jenner GA, Fryer BJ, et al. Inductively coupled plasma-mass spectrometric analysis of geological samples: a critical evaluation based on case studies. Chem Geol 1990;83:105–18.
[33] Liu Y, Hu Z, Gao S, et al. *In situ* analysis of major and trace elements of anhydrous minerals by LA-ICP-MS without applying an internal standard. Chem Geol 2008;257:34–43.
[34] Govindaraju K. 1994 compilation of working values and sample description for 383 geostandards. Geostand Geoanal Res 1994;18:1–158.
[35] Schudel G, Lai V, Gordon K, et al. Trace element characterization of USGS reference materials by HR-ICP-MS and Q-ICP-MS. Chem Geol 2015;410:223–36.
[36] Park J-W, Hu Z, Gao S, et al. Platinum group element abundances in the upper continental crust revisited – New constraints from analyses of Chinese loess. Geochim Cosmochim Acta 2012;93:63–76.
[37] Marx SK, Kamber BS. Trace-element systematics of sediments in the Murray-Darling Basin, Australia: sediment provenance and palaeoclimate implications of fine scale chemical heterogeneity. Appl Geochem 2010;25:1221–37.
[38] Sun S-S, McDonough W-S. Chemical and isotopic systematics of oceanic basalts: implications for mantle composition and processes, 42. Geol Soc Lon Spec Pub; 1989. pp. 313–345.